


Article

Fault Diagnosis and Its Applications to Fault Tolerant Control of a Turbojet Engine

Dong-Ju Han 

Department of Aircraft Maintenance Engineering, Far East University, Eumseong 27601, Republic of Korea; djhan5960@gmail.com; Tel.: +82-43-880-3842

Abstract: This paper presents a comprehensive study of model-based fault diagnosis (FD) and a fault-tolerant control (FTC) scheme for sensor and actuator faults of turbojet engines. For actuator FD, an unbiased estimation scheme with a modified Kalman filter (KF) was developed. For sensor FD, two approaches, the generalized likelihood ratio with robust KF and the pseudo actuator model with modified KF, were investigated in a comparative study. For fault detection and isolation, test statistics are commonly employed to detect fault behavior. For FTC, integral-type sliding mode control using control reconfiguration and the reconstruction of the sensor signal was adopted with the FD schemes. The effectiveness of the employed methods was demonstrated in this study and discussed with numerical simulations.

Keywords: fault diagnosis; fault-tolerant control; Kalman filter; sliding mode control; turbojet engine

1. Introduction

The safety and reliability of turbojet engines are dependent on the engine control status. Major parts in the engine control system are vulnerable to faults or failures. Fault-tolerant control (FTC) with fault diagnosis (FD) for impaired conditions of actuators and sensors can prevent or minimize this issue. Here, FD stands for fault detection and isolation (FDI) by a certain threshold level regarding the onset, as well as the location and identification of severity of any fault [1].

A significant amount research has been conducted on aircraft engine systems regarding the methodology of FD and/or FTC [1–8]. Active FTC (AFTC) requires FD information on the faults of engine parameters. In the FD of the engine system, actuator and sensor faults are addressed using the state and the parameter estimations [2,5–8], respectively, whereas engine component faults affect performance parameters such as efficiency and mass flow rate, which are estimated from the gas path analysis (GPA) [3,4]. Jinqun et al. [3–5] proposed several methods for FD and FTC of aircraft engines. FTC with proper FD can maintain performance even if an actuator or sensor is faulty. It may allow the faulty actuator or sensor to be replaced with analytical redundancy or physical replacements using FDI, guaranteeing stability and saving on operating costs [5,8].

In model-based FD and FTC methods, the robust observer [2,4,6,8–18] and Kalman filter (KF), as stochastic observer methods, are the most well-known [3,7,19–25]. In FTC methodology, passive-type FTC [8,9,14] using system robustness irrespective of FD is suitable for a limited range of faults. AFTC can address a wide range of faults, including significantly unanticipated faults [5–7,10–13,15–20,25]. For FTC laws, sliding mode control (SMC), associated with sliding mode observer (SMO), is regarded as a powerful technique due to its robustness and ability to cope with disturbances and model uncertainties [5,6,11–18]. Edwards et al. [11–13] built frameworks for FTC with SMC by developing an adaptation mechanism for actuator faults and robust fault reconstruction for sensor faults. Ebrahim et al. [14] proposed sensor FD and FTC with SMO, utilizing an optimization of the H_{∞} technique, which is similar to an adaptive control technique [8,15].



Citation: Han, D.-J. Fault Diagnosis and Its Applications to Fault Tolerant Control of a Turbojet Engine. *Energies* **2023**, *16*, 3317. <https://doi.org/10.3390/en16083317>

Academic Editors: Ali Razban and Bhaskaran Gopalakrishnan

Received: 9 March 2023

Revised: 31 March 2023

Accepted: 4 April 2023

Published: 7 April 2023



Copyright: © 2023 by the author. Licensee MDPI, Basel, Switzerland. This article is an open access article distributed under the terms and conditions of the Creative Commons Attribution (CC BY) license (<https://creativecommons.org/licenses/by/4.0/>).

In aircraft engine control, an integral action in SMC ensures rapid and accurate following of feedback signals to a reference input. This increases the robustness of the system by moving instantly to a system state on a sliding manifold, such that it spans the entire state space over the switching hyperplane by eliminating the reaching phase properly [13,15–18]. Regarding the integral-type SMC, Shen et al. [17] proposed a compensation scheme without controller reconfiguration for actuator faults, and Yabin et al. [18] proposed an estimation technique for an actuator fault deviation with augmented SMO for nonlinear systems.

For a critical sensor such as the RPM sensor in the control loop, the FD scheme that supervises the loop with FDI, whether an analytical redundancy or physical redundancy is activated, provides the information in the FTC that reconfigures the actuator or reconstructs the sensor signal [7,17,25–27]. Prakash et al. [25] presented a compensation scheme using the FD technique as a generalized likelihood ratio (GLR) with KF for sensor and actuator faults. Edoardo et al. [26] investigated switching the supervisory behavior of actuator faults and the feedback loop behavior for sensor faults. Hao et al. [27] proposed a supervisor using a pre-computed controller without an FDI scheme.

Although the works described here apply to aircraft engines and other areas, most were limited to FD or FTC in actuator or/and sensor faults. An integrated study of FD and FTC in actuator and sensor faults is still required. In this paper, based on the existing research, a comprehensive study of FD and its applications to FTC in real engines is presented. For AFTC, using a model-based method, modified and robust KF schemes were employed with statistical analysis of the fault occurrence, which is an advantage of KF over SMO for achieving accurate fault estimation. Here, other than those stochastic estimators such as extended KF, unscented KF, particle filter, and some generalized filters that are efficiently utilized for a nonlinear model, KF was adequately adopted regarded as an effective estimation scheme for a linear model employed in this work [24].

For FD schemes including FDI using test statistics, the actuator fault is addressed as an unbiased estimator with a state vector, and the estimations of sensor faults are performed using two approaches: GLR [25,28] and the pseudo actuator model (PAM) [5,12–14,16]. Here, for FTC laws, the integral-type SMC-based AFTC was adopted with an accommodation scheme for the actuator fault. For the FTC of the fault of RPM sensors in an SMC control loop, the supervisory approach was employed in conjunction with the FD scheme.

The rest of this paper is organized as follows. Section 2 presents the engine dynamics and its state space model. Section 3 investigates FD methods and integral-type SMC for FTC schemes of actuator and sensor faults in the control system of the engine. Section 4 demonstrates the simulation results to validate the effectiveness of the employed methods and schemes for this engine. Section 5 draws conclusions related to this work.

2. Mathematical Model of the Engine Control System

The target model was a one-spool turbojet engine with a 4500 N thrust level, which is shown in Figure 1a. Its mathematical model, which precisely reflects the real engine, was employed from the component characteristic data maps developed by the GPA with the component level model (CLM) [3,4,29], which is shown in Figure 1b. Detailed descriptions of the overall cycle analysis are omitted for brevity. Some primary relations peculiar to the turbojet engine are presented here.

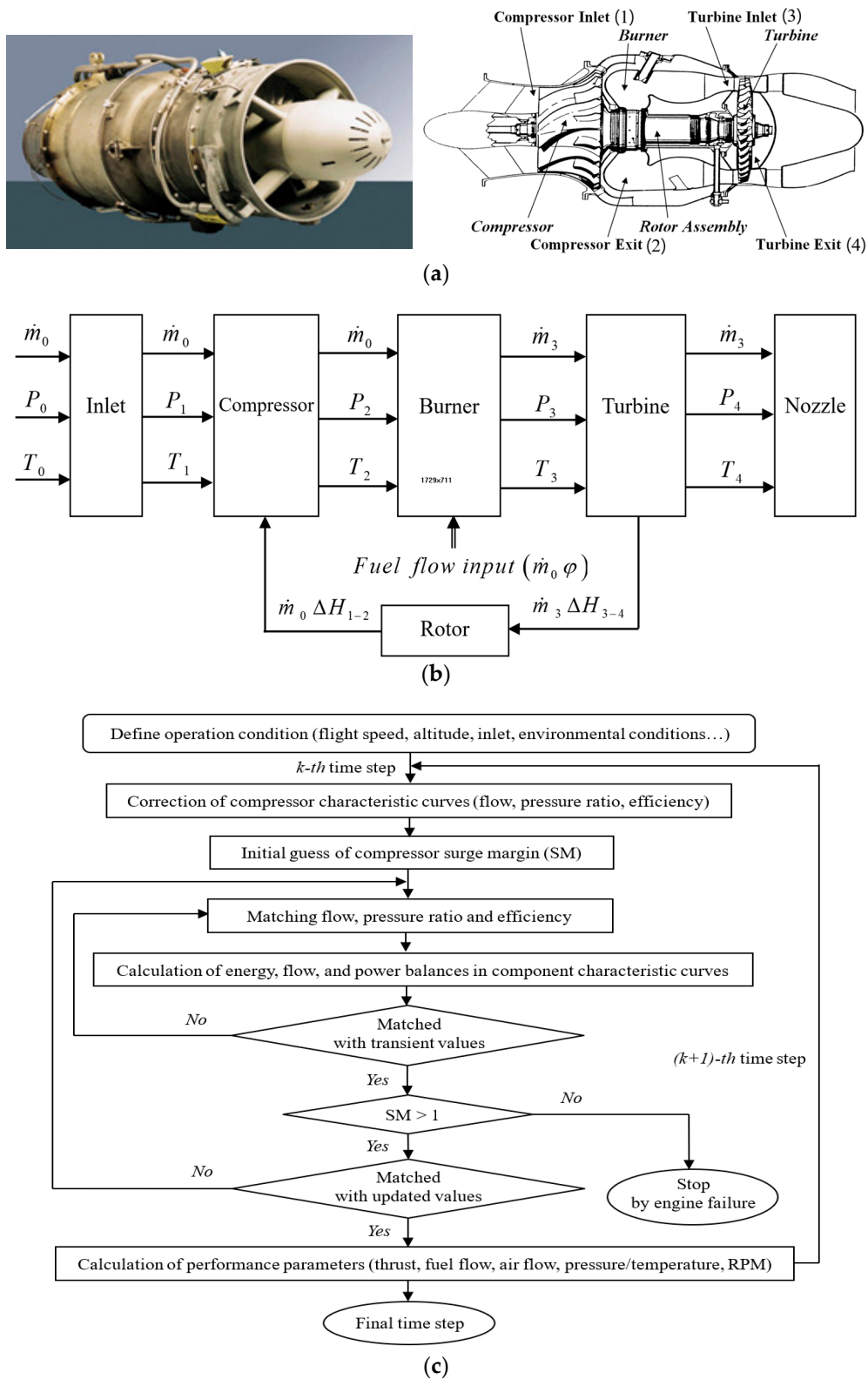


Figure 1. Schematic of the turbojet engine cycle analysis: (a) engine configuration; (b) process of gas path analysis (GPA) with component level model (CLM); (c) process of overall cycle analysis.

2.1. Steady State Thermodynamic Cycle Analysis of the Turbojet Engine

From the compressor characteristic map, the surge margin (SM) with a pressure ratio (P_2/P_1), efficiency (η_{1-2}), and normalized mass flow rate ($\dot{m}_{0*} = \dot{m}_0 \sqrt{\theta}/\delta$), is defined by

$$K_p = \frac{[\dot{m}_{0*} / (P_2/P_1)]_{op}}{[\dot{m}_{0*} / (P_2/P_1)]_{sp}} \quad (1)$$

where $\theta = T_2/288.15$, T_2 in K, $\delta = P_2/101.33$, P_2 in kPa, \dot{m}_0 denotes a mass flow rate, and subscripts "op" and "sp" denote the operating point and surge point, respectively. From the burner map, the fuel air ratio φ is given with enthalpy increase $\Delta H(T_2, T_3)$, which is a function of T_2 and T_3 , and fuel lower heating value $LHV(T_3)$, which is a function of T_3 , expressed by

$$\varphi = \frac{\Delta H(T_2, T_3)}{\eta_b LHV(T_3)} = \frac{f'(T_2, T_3)}{\eta_b} \quad (2)$$

where the superscript $'$ denotes a stoichiometric combustion process, T_3 and P_3 are obtained from the relations with normalized mass flow rate ($\dot{m}_{3*} = \dot{m}_0(1 + \varphi) \sqrt{T_3}/P_3$) and pressure drop in combustor, and the burner efficiency η_b is determined experimentally with aerodynamic load Ω , such that

$$\Omega = \frac{\dot{m}_0}{P_3^{1.8} A_3 D_3^{0.75} \exp(T_3/30)} \quad (3)$$

$$\eta_b = 1 - \Omega/100 \quad (4)$$

where A_3 and D_3 are the combustor section area and combustor linear diameter, respectively. From the turbine map, T_4 and P_4 are obtained from the relations with normalized mass flow rate ($\dot{m}_{3*} = \dot{m}_0(1 + \varphi) \sqrt{T_4}/P_4$), corrected rotational speed $N^* = N/\sqrt{T_4}$, and expansion ratio P_3/P_4 .

In a relatively a small size engine such as the turbojet engine, the boundary layer during passing through the compressor blades influential as it can change the engine performances. Hence, the compressor efficiency associated with relating parameters is corrected with the Reynolds effects, such that

$$\eta_{c\ 1-2} = \eta_{p\ 1-2\ ref} + \text{Re}_{op}/\text{Re}_{ref} (1 - \eta_{p\ 1-2\ ref}) \quad (5)$$

$$\eta_{p\ 1-2\ ref} = \log(1 + \eta_{1-2\ ref} \Delta T_{2\ ref}/T_{2\ ref}) / \log(1 + \Delta T_{2\ ref}/T_{2\ ref}) \quad (6)$$

$$\Delta T_{2\ ref} = T_{2\ ref}/\eta_{1-2\ ref} \left[(P_2/P_1)_{ref}^{\frac{\gamma_{ref}-1}{\gamma_{ref}}} - 1 \right] \quad (7)$$

where subscript "ref" represents the reference condition as sea level, 288.15 K, and 101.33 kPa, and Re_{ref} and Re_{op} denote the Reynolds numbers at the reference condition and the operating one, respectively. The turbine efficiency is corrected by the corresponding overall efficiency ($\eta_{c\ 1-2} \times \eta_{3-4}$), for which the thermodynamic cycle is reiterated with other performance parameters.

2.2. Transient Thermodynamic Cycle Analysis of the Turbojet Engine

Based on the steady state thermodynamic cycle analysis, the transient thermodynamic characteristics of the power balance, energy conservation, and flow matching conditions in each engine component were written in time-dependent forms, respectively, as follows:

$$\dot{m}_0 \Delta H_{1-2} = \dot{m}_3 \Delta H_{3-4} + (2\pi/60)^2 I_R \frac{dN}{dt} \quad (8)$$

$$\dot{m}_{o|n} H_{o|n} = \dot{m}_{i|n} H_{i|in} - C_{v, o|n} P_{o|n} V_n / (R T_{o|n}) \frac{dT_{o|n}}{dt} \quad (9)$$

$$\dot{m}_{o|n} = \dot{m}_{i|n} - V_n / (\rho_n R T_{o|n}) \frac{dT_{o|n}}{dt} \quad (10)$$

where subscripts “n”, “o”, and “i” represent the component number (shown in Figure 1a), the component output, and the component input, respectively, and I_R , R , \dot{m} , P , T , N , H , V , C_v , and ρ are the polar moment of inertia of the rotor, universal gas constant, mass flow rate, total pressure, total temperature, RPM, enthalpy, component volume, specific heat at a constant volume, and density, respectively. As shown in Figure 1c, which describes the process of the overall cycle analysis, substituting the transient thermodynamic characteristics into the steady state thermodynamic cycle analysis, the engine dynamic equations interrelated with CLM were acquired from the computation in every time step until $|K_{pc} - K_{pi}| < \varepsilon$, (K_{pi} is initial surge margin, K_{pc} is new calculated one, and ε is an admissible accuracy), with the condition $K_p > 1$, as follows

$$\dot{x}_t = f(x_t, u_t) \quad (11)$$

$$y_t = h(x_t, u_t) \quad (12)$$

where subscript t is time, $x_t = [\text{RPM}, \text{compressor exit pressure } (P_2), \text{compressor exit temperature } (T_2), \text{turbine inlet pressure } (P_3), \text{turbine inlet temperature } (T_3), \text{turbine exit pressure } (P_4), \text{turbine exit temperature } (T_4)]^T \in \mathbb{R}^n$, $y_t = [\text{RPM}, P_2, T_2, P_4, T_4]^T \in \mathbb{R}^p$ and $u_t = \text{fuel input} \in \mathbb{R}^m$ represent the state vector, measurement vector, and control input vector, respectively, and, m , n , and p denote the corresponding dimensions (here, $m = 1$, $n = 7$, $p = 5$) of u_t , x_t and y_t , respectively.

Note that the control input u_t is a fuel input driven by an actuator of engine fuel systems. Therefore, ignoring a time lag between the actuator and the fuel system, the actuator controls directly the fuel injected to the burner, which determines the operation condition of the state vector and the performance.

2.3. State Space Model of the Engine Control System

At an operating point x_0 , u_0 , substitutions of the perturbed values, while ignoring higher order terms $\Delta x_t = x_t - x_0$, $\Delta \dot{x}_t = \dot{x}_t - \dot{x}_0$, $\Delta u_t = u_t - u_0$ and $\Delta y_t = y_t - y_0$, into dynamic Equations (11) and (12), resulted in the following linear models:

$$\Delta \dot{x}_t = A \Delta x_t + B \Delta u_t \quad (13)$$

$$\Delta y_t = C \Delta x + D \Delta u_t \quad (14)$$

where subscript t is a time, $A \in \mathbb{R}^{n \times n}$, $B \in \mathbb{R}^{n \times m}$, $C \in \mathbb{R}^{p \times n}$, and $D \in \mathbb{R}^{p \times m}$ are Jacobian matrices, which can be efficiently computed from the scheme as in [30], such that applying the conditions for constant input $\Delta u = \mathbf{0}$ and equilibrium $\Delta \dot{x} = \mathbf{0}$ to $\Delta x = A^{-1} \Delta \dot{x} - A^{-1} B \Delta u$ in Equation (13), respectively, A and B are computed from $A \approx \Delta \dot{x} / \Delta x$ and $A^{-1} B \approx \Delta x / \Delta u$, respectively, and from the constant input $\Delta u = \mathbf{0}$ to $\Delta y = CA^{-1} \Delta \dot{x} - CA^{-1} B \Delta u + D \Delta u$ in Equation (14), C and D are computed from $CA^{-1} \approx \Delta y / \Delta \dot{x}$ and $D \approx \Delta y / \Delta u - C \Delta x / \Delta u$, respectively.

For real implementations, Equations (13) and (14) were transformed to the discrete state space form with time index k , omitting Δ for notational simplicity, and reflecting noise, as follows [24]:

$$x_{k+1} = \Phi x_k + \Gamma u_k + w_k \quad (15)$$

$$y_k = C x_k + D u_k + v_k \quad (16)$$

where $\Phi = \int_0^{T_s} e^{A\tau} d\tau \in \mathbb{R}^{n \times n}$, $\Gamma = \int_0^{T_s} e^{A\tau} B d\tau \in \mathbb{R}^{n \times m}$, T_s is the sampling period, $w_k \in \mathbb{R}^n \sim N(0, Q_k)$ and $v_k \in \mathbb{R}^p \sim N(0, R_k)$ are uncorrelated zero-mean Gaussian noises of process and measurement, respectively, and Q_k and R_k are the process noise covariance matrix and measurement noise covariance matrix, respectively.

3. FD and Its Applications to FTC

Figure 2 shows the proposed concept of the FTC with FD for the turbojet engine system. The following assumptions were considered for analytical convenience.

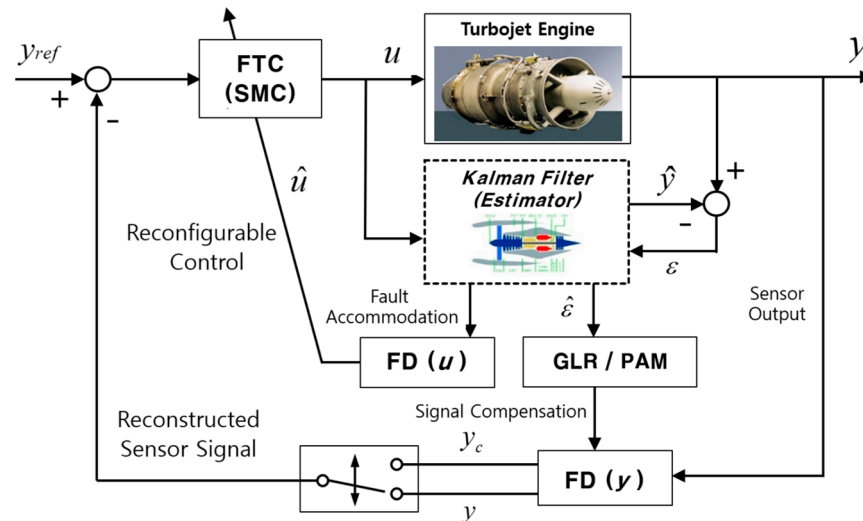


Figure 2. Schematic of fault diagnosis (FD) and fault tolerant control (FTC) with sliding mode control (SMC) in the turbojet engine control system.

Assumption 1. Only one fault in each of the actuators and sensors occurs sequentially in time, which is realistic in practical situations. Therefore, the FD and FTC of the actuator and the sensor are addressed separately.

Assumption 2. Provided that the mathematical model of the turbojet engine is described precisely and the fault estimations reflecting process noise handle some of the uncertainties of the system, we strongly assume that the modeling error and disturbance effect are not considered.

3.1. FD and FTC of the Actuator

For actuator faults, the multiplicative fault model with the control effectiveness of the control input in Equations (15) and (16) was introduced [10,19–21,25]. In order to estimate the unknown loss of the control effectiveness due to the actuator fault, we managed β_k as an additive mechanism in the control parameters, as follows:

$$x_{k+1} = \Phi x_k + \Gamma u_k + Y_{f,k} \beta_k + w_k \tag{17}$$

$$y_k = Cx_k + Du_k + \Theta_{f,k} \beta_k + v_k \tag{18}$$

where $\beta_k = \text{diag}[\beta_k^1, \beta_k^2, \dots, \beta_k^m]$, $0 \leq \beta_k^i \leq 1$ (0: no fault, 1: completely fail, partial fault elsewhere) is the i -th component of β_k , $Y_{f,k} = -\Gamma U_k \in \mathbb{R}^{n \times m}$, $\Theta_{f,k} = -D U_k \in \mathbb{R}^{p \times m}$ and $U_k = \text{diag}[u_k^1, u_k^2, \dots, u_k^m]$, where u_k^i is the i -th component of the control vector.

3.1.1. Actuator FD with Modified KF (Estimation of Control Effectiveness)

In the diagnosis of a faulty control parameter, two solution approaches have been used: a bias estimator that estimates an input fault as a parameter-wise two-stage KF [19–21], and an unbiased estimator that treats an input fault as a state vector [22,25]. In this work, the unbiased estimator approach with the control effectiveness factor is employed as a random walk process with an additive noise $w_{\beta,k} \in \mathbb{R}^m$, such that [19,21,25]

$$\beta_{\kappa+1} = \beta_{\kappa} + w_{\beta,k} \quad (19)$$

and combining these into a state parameter reduces the one state vector represented by

$$x_{x\beta,k+1} = \Phi_{x\beta,k} x_{x\beta,k} + \Gamma_{x\beta} u_k + w_{x\beta,k} \quad (20)$$

$$y_k = C_{x\beta,k} x_{x\beta,k} + D u_k + v_k \quad (21)$$

where $x_{x\beta,k} = [x_k \ \beta_k]^T$, $\Phi_{x\beta,k} = \begin{bmatrix} \Phi & Y_{f,k} \\ \mathbf{0}_{m \times m} & \mathbf{I}_{m \times m} \end{bmatrix}$, $\Gamma_{x\beta} = [\Gamma \ \mathbf{0}_{m \times m}]^T$, $w_{x\beta,k} = [w_k \ w_{\beta,k}]^T$, $C_{x\beta,k} = [C \ \Theta_{f,k}]$.

KF activates as a tracking filter to observe an unknown state parameter in Equations (20) and (21). It normally provides an optimal estimate of the state; however, if the true state is significantly different from the normal status, i.e., in the presence of an actuator fault, the state estimate may produce a poor accuracy. Such an error is tuned to forget [19,20,24]. The estimate scheme by KF is modified with tuning factor $\lambda_{|k}$, as follows:

$$P_{x\beta,k|k-1} = \lambda_{|k} \Phi_{x\beta,k} P_{x\beta,k-1|k-1} \Phi_{x\beta,k}^T + Q_{x\beta,k} \quad (22)$$

$$K_k = P_{x\beta,k|k-1} C_{x\beta,k}^T (C_{x\beta,k} P_{x\beta,k|k-1} C_{x\beta,k}^T + R_k)^{-1} \quad (23)$$

$$\hat{x}_{x\beta,k|k-1} = \Phi_{x\beta,k} \hat{x}_{x\beta,k-1|k-1} + \Gamma_{x\beta} u_{k-1} \quad (24)$$

$$\hat{x}_{x\beta,k|k} = \hat{x}_{x\beta,k|k-1} + K_k (y_k - C_{x\beta,k} \hat{x}_{x\beta,k|k-1} - D_{x\beta} u_{k-1}) \quad (25)$$

$$P_{x\beta,k|k} = (\mathbf{I} - K_k C_{x\beta,k}) P_{x\beta,k|k-1} \quad (26)$$

where $E(w_{x\beta,k}) = \mathbf{0}$ and $E(v_k) = \mathbf{0}$, $Q_{x\beta,k} = E(w_{x\beta,k} w_{x\beta,k}^T)$, and $R_k = E(v_k v_k^T)$ are uncorrelated zero-mean Gaussian process and measurement noise sequences, process noise covariance and measurement noise covariance matrices, respectively, and $E[\cdot]$ denotes a statistical expectation.

Remark 1. A proper value of $\lambda_{|k}$ will give the filter credence to the measurements with the process noise. Analytical bases to adjust the value have been suggested in [19,21,24]. However, its applications and accuracy require further study. In this work, as a direct approach, $\lambda_{|k}$ was tuned empirically with numerical simulations to ensure a good result.

For actuator FDI, the hypothesis test for whether the fault occurs is employed. The test statistics, indicating a decision measure to determine the fault occurrence, are as follows [19,20]:

$$d_{\beta,k}^i = \sum_{j=k-L+1}^k (\hat{\beta}_j^i)^2 / P_{\beta^i \text{ of } x\beta, j} \begin{matrix} H_1 \\ \geq \\ l_{\beta}^i \\ \leq \\ H_0 \end{matrix} \quad (27)$$

where $\hat{\beta}_j^i$ is the i -th component of the fault estimate $\hat{\beta}_k$, L is the window length, H_0 is the null hypothesis and means no significant fault, H_1 is the alternative hypothesis and means a significant level of loss of control effectiveness, and l_β^i and P_β^i of $x_{\beta,j|j}$ are the decision threshold and the process covariance of the control effectiveness in the i -th input channel in $P_{x_{\beta,k}|k}$, respectively.

Remark 2. The threshold determination is dependent on the significance level ($0 < \alpha < 1$), which is defined by $(P\{\chi_{d_\beta}^2(=d_{\beta,k}^i) > \chi_{l_\beta}^2(=l_\beta^i)\} = \alpha)$ of the decision reliability used with the χ^2 test. The choice of decision threshold is dependent on the window length [19,20,23]. It is a trade-off between detection delay time and estimation accuracy. As the window length increases (decreases), the estimation accuracy and the probability of a missed detection increase (decrease), but the detection speed and the probability of a false alarm decrease (increase).

3.1.2. Actuator-Fault-Tolerant SMC with Integral Action [6,11–13]

We introduced a state $e_r \in \mathbb{R}^q$, ($q \leq p$) for an integral action with output feedback in the SMC loop [13,16–18]:

$$e_r = \int_{t_0}^t (y_r - y_d) d\tau \quad (28)$$

where $y_r \in \mathbb{R}^q$ is the reference input vector and $y_d = C_d x$, where $C_d \in \mathbb{R}^{q \times n}$ represents the output distribution matrix that indicates the feedback signal components projected to the control input. Then, augmenting the additional state with $e_r = y_r - C_d x$ to Equation (20) reduces it to the discrete state space form, as follows:

$$\tilde{x}_{k+1} = \tilde{A} \tilde{x}_k + \tilde{B} \tilde{u}_k \quad (29)$$

where $\tilde{x}_k = [e_{r,k} \ x_k]^T$, $\tilde{u}_k = [y_{r,k} \ u_k]^T$, $\tilde{A} = \begin{bmatrix} \mathbf{0}_{q \times q} & -C_d \\ \mathbf{0}_{n \times n} & \Phi \end{bmatrix}$ and accommodating the loss of control effectiveness with the estimated value $\hat{\beta}_k$, such that $\hat{B} = \begin{bmatrix} \mathbf{I}_{q \times q} & \mathbf{0}_{q \times m} \\ \mathbf{0}_{n \times q} & \Gamma \hat{f}_k \end{bmatrix}$, where $\hat{f}_k = \mathbf{I}_{m \times m} - \hat{\beta}_k$.

Design of the sliding surface: We applied the new coordinates defined by $z_k = T_r \tilde{x}_k = [\tilde{x}_{1,k} \ \tilde{x}_{2,k}]^T$, where $T_r \in \mathbb{R}^{(n+q) \times (n+q)}$ is the orthogonal matrix that is computed from QR decomposition of $\tilde{B} \in \mathbb{R}^{(n+q) \times (n+m)}$. Then, Equation (29) was partitioned into the controllable canonical form with $\tilde{x}_{1,k} \in \mathbb{R}^n$ and $\tilde{x}_{2,k} \in \mathbb{R}^q$, such that:

$$\tilde{x}_{1,k+1} = \tilde{A}_{11} \tilde{x}_{1,k} + \tilde{A}_{12} \tilde{x}_{2,k} + B_r y_{r,k} \quad (30)$$

$$\tilde{x}_{2,k+1} = \tilde{A}_{21} \tilde{x}_{1,k} + \tilde{A}_{22} \tilde{x}_{2,k} + \hat{B}_2 u_k \quad (31)$$

where $B_r = [\mathbf{I}_{q \times q} \ \mathbf{0}_{(n-q) \times q}]^T$, $\hat{B}_2 \in \mathbb{R}^{q \times m}$ is the accommodated component of the matrix $T_r \hat{B}$, and $\tilde{A}_{11} \in \mathbb{R}^{n \times n}$, $\tilde{A}_{12} \in \mathbb{R}^{n \times q}$, $\tilde{A}_{21} \in \mathbb{R}^{q \times n}$ and $\tilde{A}_{22} \in \mathbb{R}^{q \times q}$ are the components of the system matrix $T_r \tilde{A} T_r^T$.

Based on this coordinate system, we considered the sliding surface $s_k = \{\tilde{x}_k \in \mathbb{R}^{n+q} : S \tilde{x}_k = S T_r^T z_k \equiv S_r y_{r,k}\}$, where $S T_r^T \triangleq [S_1 \ S_2]$, $S_1 \in \mathbb{R}^{n \times n}$, $S_2 \in \mathbb{R}^{q \times q}$, and $S_r \in \mathbb{R}^{q \times q}$ are design parameters to be determined. Here, without loss of generality, $S_2 = \mathbf{I}_{q \times q}$. Then, we imposed a condition for a controller to induce an ideal sliding motion, i.e., $s_k = S_1 \tilde{x}_{1,k} + \tilde{x}_{2,k} = \mathbf{0}$ yielded the reduced motion of the system, which took place on the sliding surface as follows:

$$\tilde{x}_{1,k+1} = (\tilde{A}_{11} - \tilde{A}_{12} S_1) \tilde{x}_{1,k} \quad (32)$$

where for the available hyperplane, the matrix pair $(\tilde{A}_{11}, \tilde{A}_{12})$ should be completely controllable, for which the necessary condition is $\text{rank} \begin{bmatrix} z\mathbf{I} - \tilde{A}_{11} & \tilde{A}_{12} \end{bmatrix} = n - q$ for all z .

Remark 3. The values S_1 in Equation (32) and S_r in the set point motion on the hyperplane can be obtained from the methods of a minimization of a cost functional with quadratic integrand or a pole assignment, among which the former is selected in this work, which is described in Appendix A.

Design of the control law: We defined a change in coordinates with states and sliding surface by $[\tilde{x}_1 \ s]^T \triangleq T_s[\tilde{x}_1 \ \tilde{x}_2]^T$ in Equations (30) and (31), where $T_s = \begin{bmatrix} \mathbf{I} & \mathbf{0} \\ S_1 & S_2 \end{bmatrix} = \begin{bmatrix} \mathbf{I} & \mathbf{0} \\ S_1 & \mathbf{I} \end{bmatrix}$ with the designed value of S_1 . Then, the coordinates of the switching hyperplane associated with the states could be represented by the following:

$$\tilde{x}_{1,k+1} = \bar{A}_{11}\tilde{x}_{1,k} + \bar{A}_{12}s_k + B_r y_{r,k} \quad (33)$$

$$s_{k+1} = \bar{A}_{21}\tilde{x}_{1,k} + \bar{A}_{22}s_k + \hat{L}_k u_k + S_1 B_r y_{r,k} \quad (34)$$

where $\bar{A}_{11} = \tilde{A}_{11} - \tilde{A}_{12}S_1 \in \mathbb{R}^{n \times n}$, $\bar{A}_{12} = \tilde{A}_{12} \in \mathbb{R}^{n \times q}$, $\bar{A}_{21} = S_1 \tilde{A}_{11} + \tilde{A}_{21} - \tilde{A}_{22}S_1 \in \mathbb{R}^{q \times n}$, $\bar{A}_{22} = S_1 \tilde{A}_{12} + \tilde{A}_{22} \in \mathbb{R}^{q \times q}$ and $\hat{L}_k = S \hat{B}_2 \in \mathbb{R}^{q \times m}$.

Based on this coordinate system, the control law was developed, consisting of two parts:

$$\hat{u}_k = u_{L,k} + u_{N,k} \quad (35)$$

where the linear part $u_{L,k}$ induces the nominal system that is stabilized by restricting it to the sliding manifold, and the nonlinear term $u_{N,k}$ develops a discontinuous switching action during the reaching phase.

The linear part is designed by substituting the condition on the sliding surface $\dot{s} = \phi(s - S_r y_r)$, where ϕ is chosen as satisfying the Lyapunov equation $P_1 \phi + \phi^T P_1 = -\mathbf{I}$ for any $P_1 > 0$, and accommodating the loss of control effectiveness with $\hat{\Lambda}_k$, which is a nonsingular diagonal matrix, as follows:

$$\begin{aligned} u_{L,k} &= \hat{\Lambda}_k^{-1} \left[-\bar{A}_{21}\tilde{x}_{1,k} - \bar{A}_{22}s_k - S_1 B_r y_{r,k} + \phi(s_k - S_r y_{r,k}) \right] \\ &= -\hat{\Lambda}_k^{-1} \left[(S \tilde{A} - \phi S) \tilde{x}_k + (\phi S_r + S_1 B_r) y_{r,k} \right] \end{aligned} \quad (36)$$

The nonlinear part $u_{N,k}$ of the sliding mode controller was designed as follows:

$$u_{N,k} = \begin{cases} -\rho_k \hat{\Lambda}_k^{-1} \frac{P_1 (s_k - S_r y_{r,k})}{\|P_1 (s_k - S_r y_{r,k})\|} & \text{if } s_k - S_r y_{r,k} \neq \mathbf{0} \\ \mathbf{0} & \text{otherwise} \end{cases} \quad (37)$$

where ρ_k is a scalar function to be chosen for adjusting a compensation of unknown uncertainties.

Remark 4. For control activity of the linear part shown in Equation (36), the first term governs the primarily control action, which is the feedback control gain, and the second term is the feedforward control gain for the reference input. The linear part overcomes most of the uncertainties in the well-designed integral controller. Furthermore, if the actuator fault is well-estimated or in fault-free condition, the nonlinear part can be ignored [6].

Theorem 1. The stability of the motion restricted to the sliding surface is guaranteed quadratically with the condition satisfying $P_2 \bar{A}_{11} + \bar{A}_{11}^T P_2 = -\mathbf{I}$ for any $P_2 > 0$, and provided that $\|y_r\| < \|\tilde{x}_1\| / (2\lambda_{\max}(P_2))$ holds.

Theorem 2. *The stability of the motion in the reaching phase is guaranteed under the premise that the scalar function ρ_t holds the following condition:*

$$\rho_t \geq \frac{\|s\|}{2\|P_2 s\|} \|S_r y_r\| + \gamma \quad (38)$$

where arbitrary constant $\gamma \geq 0$ and the reference input $\|S_r y_r\|$ on each hyperplane are bounded.

The proofs of Theorems 1 and 2 are described in Appendix B.

3.2. Sensor FD and Sensor-Fault-Tolerant SMC

Considering the control system represented by a state space equation with additive sensor faults in Equation (16), as follows:

$$x_{k+1} = \Phi x_k + \Gamma u_k + w_k \quad (39)$$

$$y_k = C x_k + D u_k + \mu_i(t) e_i \sigma(k-t) + v_k \quad (40)$$

where $\mu_i(t) \in \mathbb{R}^p$ represents the additive sensor fault occurring at time t in the i -th sensor, which is unknown but bounded $\|\mu_i(t)\| \leq \delta$, where δ is a known function, e_i is the unit vector to the i -th fault type and location, and $\sigma(k-t)$ is the unit step function, defined as 1 if $k \geq t$ and 0 if $k < t$. Note that in the engine control system, RPM, which is directly related to a fuel input, is used as the feedback sensor in the control loop.

3.2.1. GLR Approach with Robust KF

While the KF gives good estimations of the measurement parameters under normal conditions, the parameter estimations become poor in faulty conditions, which is similar to the actuator fault. In this work, a robust KF algorithm [23], which can give an accurate parameter estimation against a sensor fault, was introduced, such that the scale factor S_k was adaptively given in innovation covariance, as follows:

$$P_{x,k|k-1} = \Phi P_{x,k-1|k-1} \Phi^T + Q_k \quad (41)$$

$$\hat{x}_{k|k-1} = \Phi \hat{x}_{k-1|k-1} + \Gamma u_{k-1} \quad (42)$$

$$e_k = y_k - C \hat{x}_{k|k-1} - D u_{k-1} \quad (43)$$

$$S_k = \left(\varepsilon_k^T \varepsilon_k - \text{tr}(C P_{x,k|k-1} C^T) \right) / \text{tr}(R_k) \quad (44)$$

$$P_{y,k} = C P_{x,k|k-1} C^T + S_k R_k \quad (45)$$

$$\hat{x}_{k|k} = \hat{x}_{k|k-1} + P_{x,k|k-1} C^T P_{y,k}^{-1} \varepsilon_k \quad (46)$$

$$P_{k|k} = (\mathbf{I} - P_{x,k|k-1} C^T P_{y,k}^{-1} C) P_{k|k-1} \quad (47)$$

where $\text{tr}(\cdot)$ denotes the trace of the matrix, $E(w_k) = \mathbf{0}$ and $E(v_k) = \mathbf{0}$, $Q_k = E(w_k w_k^T)$ and $R_k = E(v_k v_k^T)$ are uncorrelated zero-mean Gaussian process and measurement noise sequences, and process noise covariance and measurement noise covariance matrices, respectively.

Remark 5. When there is no sensor fault, $S_k = 1$ is the conventional filter. In sensor faults, the KF gain is adapted by adjusting S_k for estimation robustness. A higher S_k causes a smaller KF gain in order to reduce the covariance of the faulty innovation sequence [23].

For sensor FDI, the test statistics to confirm the occurrence of a sensor fault at time t in the i -th sensor were employed in the time interval $[t, t + L]$, which followed a central χ^2 distribution with $L + 1$ degrees of freedom, as defined by the following:

$$e_{i,t} = \sum_{k=t}^{t+L} \varepsilon_k^T P_{y,k}^{-1} \varepsilon_k \begin{array}{l} H_1 \\ \geq \\ \leq \\ H_0 \end{array} l_{T,i} \quad (48)$$

where ε_k and $P_{y,k}$ are the innovation and the innovation covariance shown in Equations (43) and (45), respectively, and $l_{T,i}$ is the decision threshold in the i -th sensor.

Sensor FD with GLR algorithm: The FD scheme to find the fault magnitude and the time of occurrence in the GLR algorithm was well-described in [25,28]. For online FD with the GLR algorithm, the scheme associated with intermediate parameters was developed with the KF, which was subsequently generated in the moving window.

Considering the fault occurrence $\mu_i(t)$ with an independent function of the linear regression parameter of the state estimates and the innovations, $\hat{x}_{k|k}(t) = \mu_i(t) J_k(t) + \hat{x}(t)$, $\varepsilon_k(t) = \mu_i(t) G_k(t) + \varepsilon(t)$, where t is the time of the fault occurrence, $\hat{x}_{k|k}(t)$ and $\varepsilon_k(t)$, $\hat{x}(t)$ and $\varepsilon(t)$ are the estimated values of the states and innovations of the fault occurrence and with no fault, respectively, and $G_k(t)$ and $J_k(t)$ represent the fault signature matrix and linear regressor, respectively. Then, the test statistics to detect fault occurrence could be obtained from the recursive least square scheme, as follows:

$$l_i[t, \mu_i(t)] = \sum_{t=k+1}^L \left[\varepsilon(t)^T P_{y,k}^{-1} \varepsilon(t) - (\varepsilon(t) - \mu_i(t) G_k(t))^T P_{y,k}^{-1} (\varepsilon(t) - \mu_i(t) G_k(t)) \right] \quad (49)$$

$$= b_i(t)^T a_i(t)^{-1} b_i(t)$$

which used, for $k \geq t$

$$a_i(t) = e_i^T \sum_{k=t}^{t+L} G_k(t) P_{y,k}^{-1} G_k(t)^T e_i, b_i(t) = e_i^T \sum_{k=t}^{t+L} G_k(t) P_{y,k}^{-1} \varepsilon_k(t) \quad (50)$$

where $\varepsilon_k(t)$ is the innovations on a fault occurrence and $G_k(t)$ is obtained from the recursive process, such that we can compare the expected values of $\delta_k(t) = \hat{x}_{k|k}(t) - \hat{x}(t)$ and $\gamma_k(t) = \varepsilon_k(t) - \varepsilon(t)$, which are defined by $E[\delta_k(t)] = \mu_i(t) J_k(t) e_i$, and $E[\gamma_k(t)] = \mu_i(t) G_k(t) e_i$, respectively, with those from the KF scheme, for $k \geq t$, as follows:

$$E[\delta_k(t)] = [\mathbf{I} - K_k C] \Phi E[\delta_{k-1}(t)] + K_k \mu_i(t) e_i \sigma(k-t) \quad (51)$$

$$E[\gamma_k(t)] = -C \Phi E[\delta_{k-1}(t)] + \mu_i(t) e_i \sigma(k-t) \quad (52)$$

where $K_k = P_{x,k|k-1} C^T P_{y,k}^{-1}$ is the Kalman gain. Then, $G_k(t)$ and $J_k(t)$ for a hypothesized fault could be computed recursively during the interval $k \in [t, t + L]$

$$G_k(t) = \mathbf{I} - C \Phi J_{k-1}(t) \quad (53)$$

$$J_k(t) = \Phi J_{k-1}(t) + K_k G_k(t) \quad (54)$$

The estimations of the i -th sensor fault occurrence μ and the corresponding time k were determined from the optimal test statistics as follows:

$$\hat{\mu}_i(\hat{k}) = \operatorname{argmax}_{\mu_i} l_i[k, \hat{\mu}_i(k)] = a_i(\hat{k})^{-1} b_i(\hat{k}) \quad (55)$$

$$\hat{k}_i = \operatorname{argmax}_k l_i[k, \hat{\mu}_i(t)] \quad (56)$$

Sensor-fault-tolerant SMC: The FDI scheme in sensor FD replaces the faulty sensor by switching over to another available sensor [15–27]. If the RPM sensor is faulty, a compensation scheme is employed in the SMC loop. The SMC with integral action leads the measurement output to the reference input, resulting in an offset from the reference input. Thus, the modification to eliminate this offset in the i -th faulty sensor is straightforward, such that the faulty measured output y_k is reconstructed in the following form:

$$y_{c,k} = y_k - \hat{\mu}_i(\hat{k}) e_i \quad (57)$$

where $y_{c,k}$ represents the compensated or corrected measurement vector.

Remark 6. *If the estimation is accurate, the feedback sensor enters an unbiased state in the controller, whereby the reconstruction of the measurement output provides a redundant activity. In that case, this sensor FD could be used as a virtual sensor without the need for FDI activity [2,4,5,12,13,16].*

3.2.2. PAM Approach with Modified KF

Provided that the sensor is a low pass filter, we can introduce a new state x_f that is an alternative variable of y , satisfied as follows [5,12–14,16]:

$$\begin{aligned} x_{f,k+1} &= -A_f x_{f,k} + A_f y_k \\ &= -A_f x_{f,k} + A_f C x_k + A_f D u_k + A_f \tau_k \sigma(k-t) \end{aligned} \quad (58)$$

where $A_f \in \mathbb{R}^{p \times p}$ is a design parameter, typically denoted as an inverse of the time constant, which is a positive and stable matrix. Combining Equations (39) and (58) with the sensor fault term denoted by τ_k , an augmented state-space system of order $n+p$ can be built as follows:

$$z_{f,k+1} = \bar{A}_f z_{f,k} + \bar{B}_f u_k + F \tau_k + w_{f,k} \quad (59)$$

where $z_f = [x \ x_f]^T$, $\bar{A}_f = \begin{bmatrix} \Phi & \mathbf{0} \\ A_f C & -A_f \end{bmatrix}$, $\bar{B}_f = [\Gamma \ A_f D]^T$, $F = [\mathbf{0} \ A_f]^T$, $w_{f,k} = [w_{x,k} \ w_{x_f,k}]^T$.

Sensor FD with PAM: We managed the sensor fault τ_k as a random walk model with an additive noise, such that

$$\tau_{k+1} = \tau_k + w_{\tau,k} \quad (60)$$

where $w_{\tau,k} \in \mathbb{R}^p$ represents zero mean Gaussian white noise sequences with known covariance vectors. Then, combining the additional state that is regarded as the sensor fault into Equation (59), the augmented state model was constructed in the following form:

$$x_{z\mu,k+1} = \tilde{A}_f x_{z\mu,k} + \tilde{B}_f u_k + w_{z\mu,k} \quad (61)$$

$$y_{f,k} = C_p x_{z\mu,k} + A_f D u_k \quad (62)$$

where $x_{z\tau} = [z_f \ \tau]^T$, $\tilde{A}_f = \begin{bmatrix} \tilde{A}_f & F \\ \mathbf{0} & \mathbf{I} \end{bmatrix}$, $\tilde{B}_f = [\tilde{B}_f \ \mathbf{0}]^T$, $C_p = [\mathbf{I}_p \ \mathbf{0}]$, $\mathbf{I}_p = [\mathbf{0} \ \mathbf{I}]$, $w_{z\tau,k} = [w_{f,k} \ w_{\tau,k}]^T$.

The sensor FD was obtained from the modified KF scheme as in the actuator faults given in Equations (22)–(26). For sensor FDI, the test statistics $d_{\tau,k}^i$ were used to indicate the decision of the fault occurrence, as follows:

$$d_{\tau,k}^i = \sum_{j=k-L+1}^k (\hat{\tau}_j^i)^2 / P_{\tau \text{ of } f, j|j}^i \begin{matrix} \geq \\ \leq \end{matrix} \begin{matrix} H_1 \\ H_0 \end{matrix} \quad l_{\tau,i} \tag{63}$$

where $\hat{\tau}_j^i$ and $P_{\tau \text{ of } f, j|j}^i$ are the i -th components of the fault estimate $\hat{\tau}_k$ and the i -th components of the covariance matrix $P_{\tau \text{ of } f}^i$ with the j -th diagonal component, respectively, and $l_{\tau,i}$ is the decision threshold in the i -th sensor.

Sensor-Fault-Tolerant SMC: The faulty measured output y_k was reconstructed as the compensated measurement vector $y_{c,k}$, such that:

$$y_{c,k} = y_k - \hat{\tau}_k \tag{64}$$

Remark 7. The matrix \mathbf{A}_f in PAM, which is conveniently in diagonal form, is a design parameter to adjust the stability and the transient performance, whereas the window length in the GLR approach determines the transient performance irrespective of the stability. For a detection delay, the GLR approach is slightly more advantageous because the time lag in PAM is inherently defective, which will be seen from the simulation results.

4. Simulation Result and Discussion

Simulations to determine the effectiveness of the proposed FD and its applied FTC of the engine were performed at sea level static and under operation conditions of RPM: 27,000 rpm, P_2 : 3365 Pa, T_2 : 167 K, P_3 : 2976 Pa, T_3 : 871 K, P_4 : 1643 Pa, and T_4 : 743 K. Under these operation conditions, the matrices in the state space model and output distribution matrix (one feedback parameter with RPM, i.e., $q = 1$) are given as follows:

$$A = \begin{bmatrix} 4.9 & -1025.8 & 492.3 & 096.0 & -55.1 & -39.6 & -13.3 \\ 171.9 & 2545.0 & -6305.5 & -15,076.0 & 1,681.8 & 960.8 & 214.6 \\ 13.7 & -134.7 & -881.6 & 118.2 & 13.0 & 10.3 & 7.8 \\ -240.9 & 50,836.0 & -38,773.0 & -53,241.0 & 4494.3 & -121.4 & 7218.7 \\ -10.6 & 4132.8 & -2791.6 & -4518.2 & -241.5 & 37.1 & 78.3 \\ 1099.9 & -289,410.0 & 227,480.0 & 308,400.0 & -29,097.0 & -10,735.0 & 2011.6 \\ 146.1 & -39,549.0 & 32,277.0 & 41,596.0 & 3174.6 & -456.4 & -7663.5 \end{bmatrix}, C = \begin{bmatrix} 1 & 0 & 0 & 0 & 0 & 0 & 0 \\ 0 & 1 & 0 & 0 & 0 & 0 & 0 \\ 0 & 0 & 1 & 0 & 0 & 0 & 0 \\ 0 & 0 & 0 & 0 & 1 & 0 & 0 \\ 0 & 0 & 0 & 0 & 0 & 1 & 0 \end{bmatrix}$$

$$B = [-158.1 \ 724.8 \ -9.48 \ 9164.2 \ 5106.6 \ -5,1825 \ -732.2]^T, D = \begin{bmatrix} -0.3 \\ -0.05 \\ -0.003 \\ -0.02 \\ 0.003 \end{bmatrix}, C_d = [1 \ \mathbf{0}_{1 \times 6}]. \tag{65}$$

In the simulations, the time step was 0.01 s, the window length was 5, and the RPM command of two step inputs was scheduled as 27,000 → 28,000 → 27,500 at 2 s and 15 s, respectively. For the noise characteristics, Gaussian noise with zero mean and standard deviations of 0.0004 (percent nominal value) were imposed equally on the process and the measurements. The design parameters were chosen with simulations of $\lambda_k = 0.9$, which was trially adjusted, $Q_k = \text{diag}[1 \ 0.4 \ \mathbf{I}_{1 \times 7}]$, $A_f = 0.45\mathbf{I}_{5 \times 5}$, $\rho_t = 1$ and $\phi = -6000$, which were adjusted within the design limits. The threshold levels in FD are commonly chosen as 1000.

4.1. FD and FTC for an Actuator Fault

In this simulation, actuator faults were arbitrarily imposed as two steps with 50% and 20% losses of control effectiveness at 7 s and 23 s, respectively. The Gaussian noise in the control effectiveness factor was empirically chosen with a zero mean and standard deviation of 0.02 (% fault value).

Figure 3a,b presents the effectiveness of the proposed FD method by showing good tracking performances with a small detection delay of FDI, as shown in the magnified views. Estimation deviations associated with very small detection time delays (about 0.01 s) between the estimated value and the real fault can be seen in the figures, which show the transient overshoots such as outliers. These outliers are unavoidable because complete synchronous detection without time delay is impossible in practice, which reflects the control reconfiguration of FTC. Figure 3b represents the FDI performance, showing that the test statistics value far exceeded the threshold value, and that its detection delay at the first fault (see the magnified view) was negligible. In this case, the significance level was so small that the possibility of a false alarm H_1 was nearly zero.

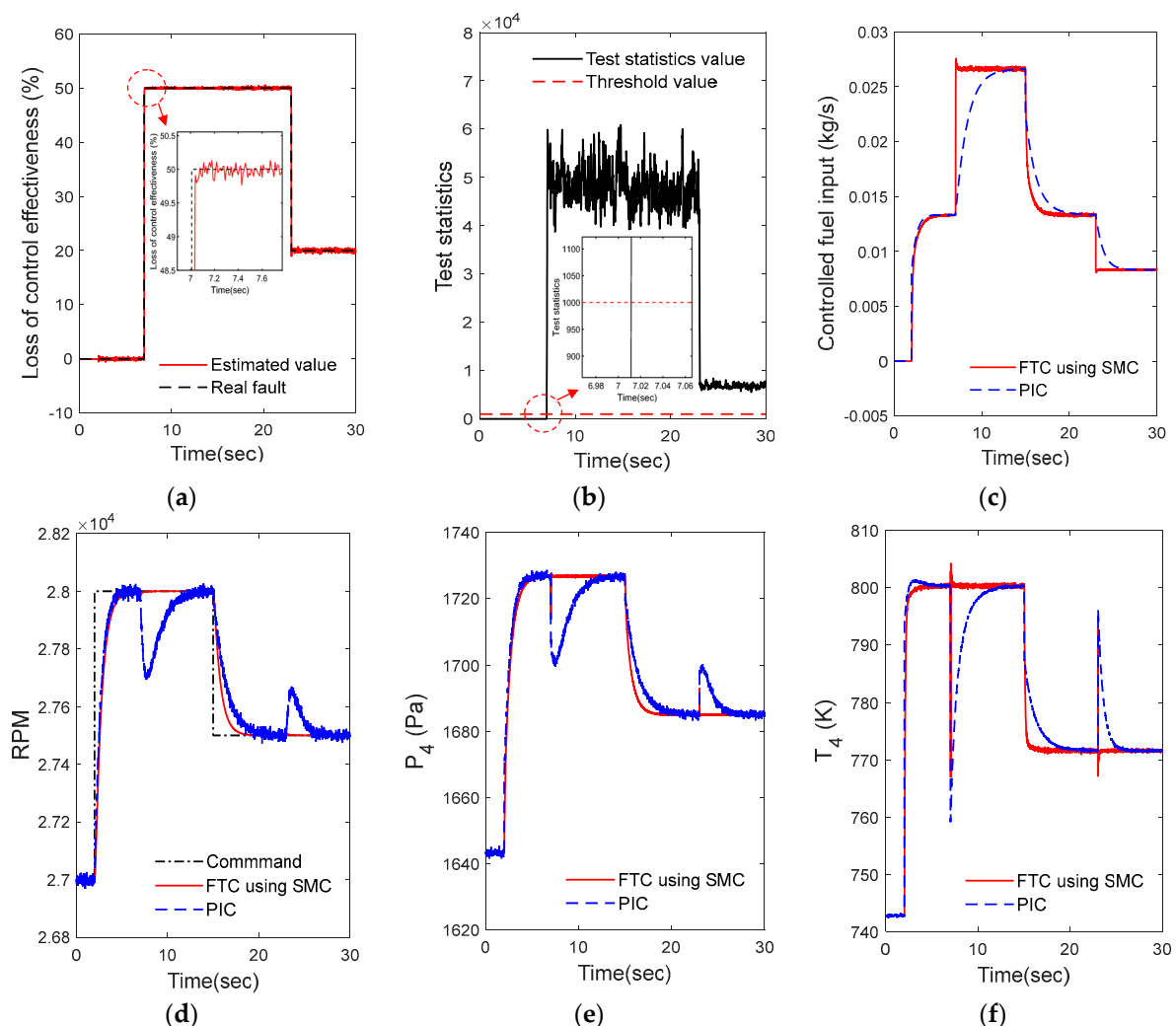


Figure 3. Simulation results: FD and FTC of an actuator fault compared with PI control (PIC): (a) fault estimation; (b) fault detection and isolation (FDI) using test statistics; (c) control reconfiguration; (d) RPM in the SMC loop; (e) response in the sensor (P_4); (f) response in the sensor (T_4).

In Figure 3c–f, the proposed FTC using SMC was compared with a well-designed conventional proportional-integral controller (PIC) that is activated following the RPM signal to RPM demand without a reconfigurable scheme for the actuator fault, where the

proportional and integral gains of the RPM feedback in the control loop are empirically chosen as a simple approach by numerical simulations, as 8.0×10^{-6} and 2.0×10^{-5} , respectively. In the no fault condition, SMC showed more or less better performances with more rapid responses than PIC. For actuator fault occurrences, FTC with SMC showed an obviously excellent performance over PIC by accommodating the fault instantly and accurately, along with some noise suppression. In Figure 3d–f, at the instants of the actuator faults, PIC resulted in quantitatively large and long fluctuations due to the impromptu controller output response, as shown in Figure 3c, whereas the proposed FTC showed robust performances without fluctuations against the faults, which can be identified from the prompt controller response, as shown in Figure 3c. Here, small switching actions are thought of as dithering motions in the reaching mode for system robustness, and due to the outliers induced by the FD process in the transient status, as shown in Figure 3c, and small overshoots appear as single outliers, as shown in Figure 3e,f. However, the RPM in the SMC loop shown in Figure 3d indicates no overshoot. The outliers here were trivial, with no dangerous effect to the system. On the other hand, the heavy fluctuations in Figure 3d–f due to PIC in the actuator fault may cause dangerous situations, such as a thermal shock or even a compressor stall, due to an abruptly low surge margin. Output parameters P_2 and T_2 were omitted because their trends were similar to P_4 in Figure 3f and T_4 in Figure 3g, respectively.

4.2. FD and FTC for Sensor Faults

For the simulations of sensor faults, two bias faults with 2% and 1% from each sensor were imposed consecutively at 7 s and 23 s, respectively. The FTC against the fault of the RPM sensor in the SMC loop is separately addressed in Figure 4, and the FD of the other sensor faults are addressed in Figure 5. Figure 4 shows fairly good FD and FTC performance for the RPM sensor fault. In Figure 4a, both approaches demonstrate good results, confirmed by the magnified view. In Figure 4b, both approaches show excellent FDI capabilities. From the magnified view, the GLR approach achieved a slightly more rapid detection speed compared with PAM, which can be also found in Figure 4a, associated with the estimation accuracy. Here, at the instances of the fault occurrences, the estimation deviations were larger than those of the actuator fault in the FD performances; however, as indicated in Figure 4c–f, the fluctuations in FTC were small due to attenuation by the signal reconstruction in the case of an actuator fault with some peaks. Those fluctuations, whose effects are trivial, are inevitable in FDI during supervisory switching action and if the faulty sensor is not virtually replaced with the estimated value [5,12]. Figure 4e,f indicates the FTC results of the measurements. Here, for a comparative study of each method for FD, the performance measure J_{est} to estimate accuracy in a quantitative manner proved the validation of the sensor FTC, defined by:

$$J_{est} = \sqrt{\frac{1}{n} \sum_{i=1}^n (\text{Real fault}_i - \text{Estimated value}_i)^2} \quad (66)$$

where i denotes the corresponding parameter and n is the number of samples. Table 1 presents the computed results from 50 Monte Carlo simulations based on Equation (65). As shown in the table, the GLR approach resulted in better accuracies over PAM, with minor differences.

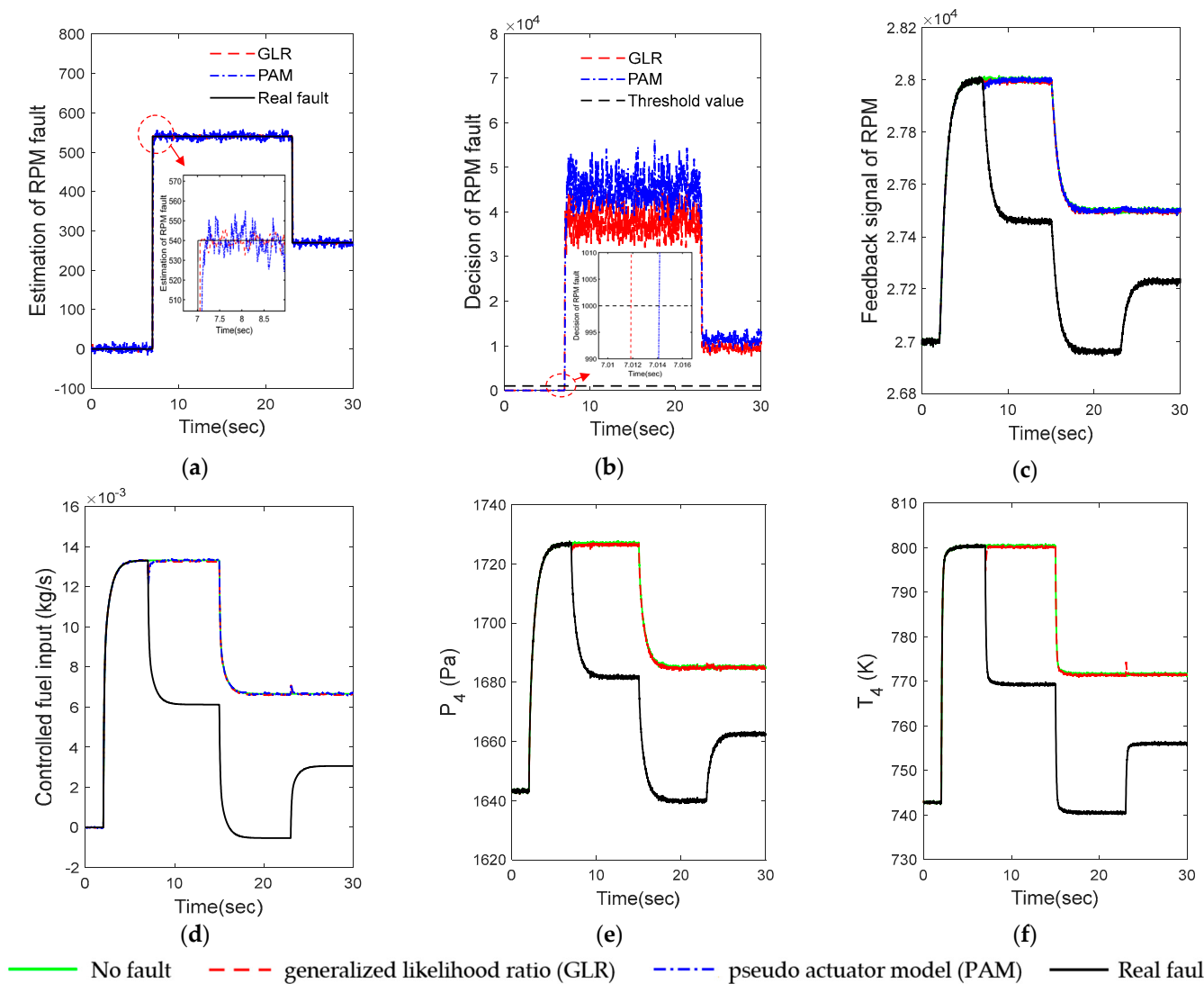


Figure 4. Simulation results: FD and FTC of the RPM sensor fault: (a) fault estimation; (b) FDI using test statistics; (c) control reconfiguration; (d) RPM in the SMC loop; (e) response in the sensor (P_4); (f) response in the sensor (T_4).

Table 1. Estimation performance measure J_{est} .

Method	RPM	P_2	T_2	P_4	T_4	CFI ¹
GLR	2.757 (0.299)	0.593 (0.061)	0.036 (0.004)	0.290 (0.023)	0.413 (0.017)	7.1×10^{-5} (3.6×10^{-6})
PAM	3.963 (0.265)	0.846 (0.054)	0.051 (0.003)	0.403 (0.022)	0.545 (0.024)	9.6×10^{-5} (4.3×10^{-6})

(): Standard deviation, ¹ Controlled Fuel Input.

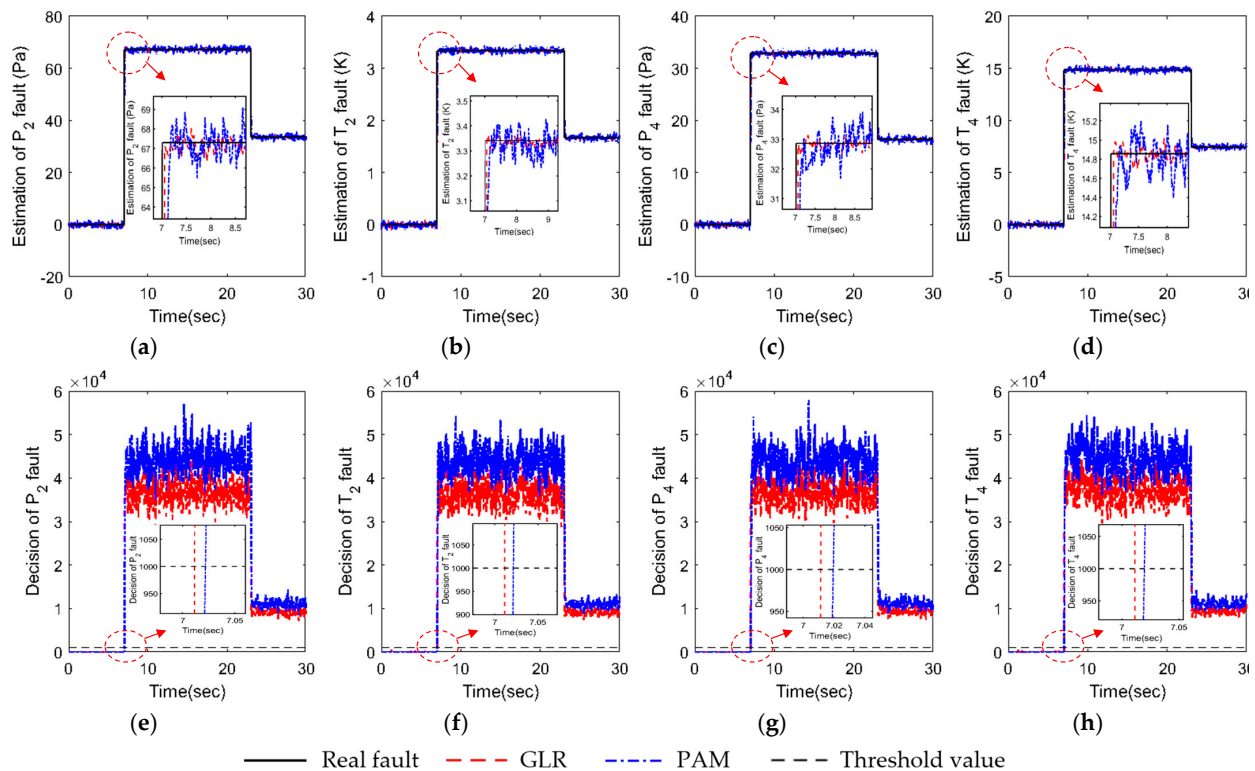


Figure 5. Simulation results: FD of the sensor faults: (a) fault estimation of P_2 ; (b) fault estimation of T_2 ; (c) fault estimation of P_4 ; (d) fault estimation of T_4 ; (e) FDI of P_2 ; (f) FDI of T_2 ; (g) FDI of P_4 ; (h) FDI of T_4 .

The FD results of other sensor faults, except the RPM sensor, are presented in Figure 5. To save space, all cases of a single fault in each sensor were given in one figure by omitting figures of the unfaulted sensors. Figure 5a–h shows good estimates of FD and FDI performances, respectively, as confirmed by the magnified views. In the figures, the values of the test statistics far exceeded the threshold levels with fast detection speeds, with no possibility of false alarms. In Figure 5a–d, both approaches demonstrate excellent estimation results for each sensor fault, which validated the effectiveness of the proposed FD methods. The GLR approach had a slightly more rapid detection speed and better accuracy than PAM.

5. Conclusions

In this paper, the methods of the model-based FD and its applications in FTC for sensor and actuator of the turbojet engine were investigated.

For the mathematical model that precisely reflects the existing turbojet engine, using the steady state and transient thermodynamic cycle analyses based on the component characteristic data maps developed by the GPA with the CLM, the state space model in discrete form for the real implementation was derived. For actuator FD of a multiplicative fault, based on a stochastic observer as a fault estimation, a modified Kalman filter scheme associated with an unbiased estimator from a combined random walk model was developed as a direct approach to identify a fault. For the sensor FD, a comparative study was performed with two approaches: GLR method with a robust KF scheme that is effectively used with the measurement parameter itself, and the method using PAM with a modified KF scheme such that the sensor fault is treated as the actuator fault by replacing a state parameter using a low pass filter scheme. In the case of FDI, the detection measure decided by the threshold level with test statistics based on the hypothesis of fault occurrence was commonly employed in both cases of FDs. For AFTC, the control law was adopted by integral-type SMC with the FD of the actuator fault and the fault of the RPM sensor in the

SMC loop. The actuator FD was used for controller reconfiguration by accommodating the actuator fault, and the sensor FD was used for the reconstruction of the sensor signal by compensating for the RPM sensor fault. The effectiveness of the employed methods was proven by numerical simulations that demonstrated fairly good FD and FTC performances against the actuator and RPM sensor faults, with some noise attenuations. In the FD of sensor faults, both approaches showed excellent performances, though the GLR approach obtained slightly more accurate results than PAM.

Future research is expected to extend to the FTC with FD using nonlinear KF or SMO in nonlinear engine model including uncertainties and disturbances.

Data Availability Statement: Not applicable.

Conflicts of Interest: The author declares no conflict of interest.

Nomenclature

AFTC	Active Fault Tolerant Control
CLM	Component Level Model
FD	Fault Diagnosis
FDI	Fault Detection and Diagnosis
FTC	Fault Tolerant Control
GPA	Gas Path Analysis
GLR	Generalized Likelihood Ratio
KF	Kalman Filter
LHV	Lower Heating Value
PAM	Pseudo Actuator Model
RPM	Revolution Per Minute
SM	Surge Margin
SMC	Sliding Model Control
SMO	Sliding Model Observer
P	pressure
T	temperature
N	RPM
R	universal gas constant
H	enthalpy
V	component volume
φ	fuel air ratio
Re	Reynolds number
I_R	rotor polar moment of inertia
C_v	specific heat at a constant volume
ρ	density
η	efficiency
\dot{m}	true mass flow rate
\dot{m}^*	normalized mass flow rate
A, B, C, D	system matrices
Φ	discrete form of A
Γ	discrete form of B
Q	process noise covariance
R	measurement noise covariance
x	state vector
y	measurement vector
u	control input vector
v	measurement noise
w	process noise
L	window length
β	control effectiveness factor
H_0	null hypothesis
H_1	alternative hypothesis

Appendix A

The values S_1 in Equation (23) and S_r were obtained from a minimization technique with linear quadratic regular. Based on the detailed derivations given in [11], S_1 and S_r were designed, respectively, as follows:

$$S_1 = Q_{22,k}^{-1} (\tilde{A}_{12}^T P_{1,k} + Q_{21,k}) \quad (\text{A1})$$

$$S_r = -K_r^{-1} B_r^T \tilde{A}_{11}^{-1} B_r \quad (\text{A2})$$

where $Q_{21,k}$ and $Q_{22,k}$ are the components of $T_r Q_k T_r^T = \begin{bmatrix} Q_{11,k} & Q_{12,k} \\ Q_{21,k} & Q_{22,k} \end{bmatrix}$, $K_r = B_r^T \tilde{A}_{11}^{-1} \tilde{A}_{12}$, Q_k is the symmetric positive definite matrix to be chosen, and $P_{1,k}$ is the unique and positive definite solution that can be obtained from the recursive discrete-time Riccati equation, such that [24]:

$$P_{1,k} = (\hat{A}_k - \tilde{A}_{12} L_k)^T P_{1,k+1} (\hat{A}_k - \tilde{A}_{12} L_k) + \hat{Q}_k + L_k^T Q_{22,k} L_k \quad (\text{A3})$$

$$L_k = (Q_{22,k} + \tilde{A}_{12}^T P_{1,k+1} \tilde{A}_{12})^{-1} \tilde{A}_{12}^T P_{1,k+1} \hat{A}_k \quad (\text{A4})$$

where $\hat{Q}_k = Q_{11,k} - Q_{12,k} Q_{22,k}^{-1} Q_{21,k}$ and $\hat{A}_k = \tilde{A}_{11} - \tilde{A}_{12} Q_{22,k}^{-1} Q_{21,k}$.

Appendix B

Proof of Theorem 1. Introducing the Lyapunov function given in a continuous form as $V_{\tilde{x}_1} = \tilde{x}_1^T P_2 \tilde{x}_1$ in Equation (33), and substituting the condition of the sliding surface $s_k = 0$ satisfies the stability condition, such that:

$$\begin{aligned} \dot{V}_{\tilde{x}_1} &= -\tilde{x}_1^T \tilde{x}_1 + 2\tilde{x}_1^T P_2 y_r \\ &\leq -\tilde{x}_1^T \tilde{x}_1 + 2\|P_2 \tilde{x}_1\| \|y_r\| \\ &\leq -\|\tilde{x}_1\|^2 + 2\lambda_{\max}(P_2)\|\tilde{x}_1\| \|y_r\| \\ &= -\|\tilde{x}_1\| \lambda_{\max}(P_2) \left(\frac{\|\tilde{x}_1\|}{\lambda_{\max}(P_2)} - 2\|y_r\| \right) < 0 \end{aligned} \quad (\text{A5})$$

□

Proof of Theorem 2. Introducing the Lyapunov function given by a continuous form as $V_s = s^T P_2 s$ in Equation (34) satisfies the stability condition as follows:

$$\begin{aligned} \dot{V}_s &= \dot{s}^T P_2 s + s^T P_2 \dot{s} \\ &= -s^T s + s^T S_r y_r - 2\rho_t \frac{s^T P_2}{\|P_2(s - S_r y_r)\|} [P_2(s - S_r y_r)] \\ &\leq -\|s\|^2 - 2\rho_t \|P_2 s\| + \|s\| \|S_r y_r\| \\ &= -\|s\|^2 - 2\|P_2 s\| \left(\rho_t - \frac{\|s\|}{2\|P_2 s\|} \|S_r y_r\| \right) < 0 \end{aligned} \quad (\text{A6})$$

□

Funding: This work was supported by the 2022 Far East University Research Grant (FEU2022S06).

References

1. Amare, D.F.; Aklilu, T.B.; Syed, I.G.; Konstantinos, G.K. A Review on Gas Turbine Gas-Path Diagnostics: State-of-the-Art Methods, Challenges and Opportunities. *Aerospace* **2019**, *6*, 83. [[CrossRef](#)]
2. Rahme, S.; Meskin, N. Adaptive sliding mode observer for sensor fault diagnosis of an industrial gas turbine. *Control Eng. Pract.* **2015**, *38*, 57–74. [[CrossRef](#)]
3. Feng, L.; Hongfei, J.; Jinqian, H. An improved extended Kalman filter with inequality constraints for gas turbine engine health monitoring. *Aerosp. Sci. Tech.* **2016**, *58*, 36–47. [[CrossRef](#)]
4. Xiaodong, C.; Jinqian, H. Health Parameter Estimation with Second-Order Sliding Mode Observer for a Turbofan Engine. *Energies* **2017**, *10*, 1040. [[CrossRef](#)]
5. Xiaodong, C.; Jinqian, H.; Feng, L. Sensor Fault Tolerant Control for Aircraft Engines Using Sliding Mode Observer. *Energies* **2019**, *12*, 4109. [[CrossRef](#)]
6. Yuan, Y.; Tianhong, Z.; Zhonglin, L.; Zhiwen, Z.; Xinglong, Z. Active fault tolerant Control of Variable Cycle Engine Using Sliding Mode Control Scheme. *Actuators* **2021**, *10*, 24. [[CrossRef](#)]
7. Amin, M.; Karim, S. Fault Tolerant Control of an Industrial Gas Turbine Based on a Hybrid Fuzzy Adaptive Unscented Kalman Filter. *ASME J. Eng. Gas Turbines Power* **2013**, *135*, 122501. [[CrossRef](#)]
8. Yan, H.M.; Xian, D.; Xi, M.S.; Fang, J.Z. Active fault tolerant tracking control of turbofan engine based on virtual actuator. *ISA Trans.* **2021**, *122*, 247–259. [[CrossRef](#)]
9. Chen, L.; Li, X.; Xiao, W.; Li, P.; Zhou, Q. Fault-tolerant Control for Uncertain Vehicle Active Steering Systems with Time-delay and Actuator Fault. *Int. J. Control Autom. Sys.* **2019**, *17*, 2234–2241. [[CrossRef](#)]
10. Yawei, W.; Lina, Y. Fault Diagnosis and Fault Tolerant Control for Manipulator with Actuator Multiplicative Fault. *Int. J. Control Autom. Sys.* **2021**, *19*, 980–987. [[CrossRef](#)]
11. Edwards, C.; Spurgeon, S.K. *Sliding Mode Control: Theory and Applications*; Taylor & Francis Ltd.: Padstow, UK, 1998; Chapter 4; ISBN 0-7484-0601-8.
12. Edwards, C.; Tan, C.P. Sensor fault tolerant control using sliding mode observers. *Control Eng. Pract.* **2006**, *14*, 897–908. [[CrossRef](#)]
13. Alwi, H.; Edwards, C. Fault Detection and Fault-Tolerant Control of a Civil Aircraft Using a Sliding-Mode-Based Scheme. *IEEE Trans. Control Sys. Technol.* **2008**, *16*, 499–510. [[CrossRef](#)]
14. Ebrahim, S.; Adnan, U.K.; Muhammad, L.; Ahmad, S.; Ghulam, H.; Athar, W.; Fahad, R.A.; Zahid, U. Sensor Fault-Tolerant Control of Microgrid Using Robust Sliding-Mode Observer. *Sensors* **2022**, *22*, 2524. [[CrossRef](#)]
15. Ming, L.; Peng, S. Sensor fault estimation and tolerant control for Itô stochastic systems with a descriptor sliding mode approach. *Automatica* **2013**, *49*, 1242–1250. [[CrossRef](#)]
16. Zhilu, Z.; Benxian, X. Sensor Fault Diagnosis and Fault Tolerant Control for Forklift Based on Sliding Mode Theory. *IEEE Access* **2020**, *8*, 84858–84866. [[CrossRef](#)]
17. Shen, Q.; Wang, D.; Zhu, S.; Poh, E.K. Integral-Type Sliding Mode Fault-Tolerant Control for Attitude Stabilization of Spacecraft. *IEEE Trans. Autom. Control* **2015**, *23*, 1131–1138. [[CrossRef](#)]
18. Yabin, G.; Jianxing, L.; Guanghui, S.; Ming, L.; Ligang, W. Fault deviation estimation and integral sliding mode control design for Lipschitz nonlinear systems. *Syst. Control Lett.* **2019**, *123*, 8–15. [[CrossRef](#)]
19. Wu1, N.E.; Zhang, Y.; Zhou, K. Detection, estimation, and accommodation of loss of control effectiveness. *Int. J. Adapt. Control Signal Process* **2000**, *14*, 775–795.
20. Zhang, Y.M.; Jiang, J. Active fault-tolerant control system against partial actuator failures. *IEE Proc.* **2002**, *149*, 95–104. [[CrossRef](#)]
21. Hsieh, C.S. Robust Two-Stage Kalman Filters for Systems with Unknown Inputs. *IEEE Trans. Auto. Con.* **2000**, *45*, 2374–2378. [[CrossRef](#)]
22. Steven, G.; Bart, D.M. Unbiased minimum-variance input and state estimation for linear discrete-time systems. *Automatica* **2007**, *43*, 111–116. [[CrossRef](#)]
23. Hajiyev, C.; Gulerand, D.C.; Hacizade, U. Two-Stage Kalman Filter for Fault Tolerant Estimation of Wind Speed and UAV Flight Parameters. *Meas. Sci. Rev.* **2020**, *20*, 35–42. [[CrossRef](#)]
24. Simon, D. *Optimal State Estimation: Kalman, H ∞ and Nonlinear Approaches*; John Wiley & Sons, Inc.: Hoboken, NJ, USA, 2006; ISBN 100-471-70858-5.
25. Prakash, J.; Sachin, C.P.; Shankar, N. A Supervisory Approach to Fault-Tolerant Control of Linear Multivariable Systems. *Ind. Eng. Chem. Res.* **2002**, *41*, 2270–2281. [[CrossRef](#)]
26. Edoardo, M.; Tommaso, A. Switching supervisory control based on controller falsification and closed-loop performance inference. *J. Process Control* **2002**, *12*, 457–466.
27. Hao, Y.; Bin, J.; Vincent, C.; Lingli, L. Supervisory Fault Tolerant Control with Integrated Fault Detection and Isolation: Switched System Approach. *Int. J. Appl. Math. Com. Sci.* **2012**, *22*, 87–97. [[CrossRef](#)]
28. Fariborz, K.; Jagadeesan, P.; Sirish, L.S. An Alternative Approach to Implementation of the Generalized Likelihood Ratio Test for Fault Detection and Isolation. *IEC Res.* **2013**, *52*, 12482–12489. [[CrossRef](#)]

29. Han, D.J. A Study on Application of Fuzzy Adaptive Unscented Kalman Filter to Nonlinear Turbojet Engine Control. *Int. J. Aeronaut. Space Sci.* **2018**, *19*, 399–410. [[CrossRef](#)]
30. Sellers, J.F.; Daniele, C.J. DYGABCD—A Program for Calculating Linear A, B, C, and D Matrices from a Nonlinear Dynamic Engine Simulation. In *NASA/TP-1295*; National Aeronautics and Space Administration, Scientific and Technical Information Office: Hampton, VA, USA, 1978.

Disclaimer/Publisher’s Note: The statements, opinions and data contained in all publications are solely those of the individual author(s) and contributor(s) and not of MDPI and/or the editor(s). MDPI and/or the editor(s) disclaim responsibility for any injury to people or property resulting from any ideas, methods, instructions or products referred to in the content.